Nanoconfinement of Molecular Magnesium Borohydride Captured in a Bipyridine-Functionalized Metal–Organic Framework

Andreas Schneemann,[†] Liwen F. Wan,[§] Andrew S. Lipton,[⊥] Yi-Sheng Liu,[‡] Jonathan L. Snider,[†] Alexander A. Baker,[§] Joshua D. Sugar,[†] Catalin D. Spataru,[†] Jinghua Guo,[‡] Thomas S. Autrey,[⊥] Mathias Jørgensen,[†,∇] Torben R. Jensen,[∇] Brandon C. Wood,[§] Mark D. Allendorf[†]* and Vitalie Stavila[†]*

† Sandia National Laboratories, 7011 East Avenue, Livermore, CA 94550, United States

§ Lawrence Livermore National Laboratory, 7000 East Avenue, Livermore, CA 94550, United States

⊥ Pacific Northwest National Laboratory, Richland WA 99354, United States

‡ Advanced Light Source, Lawrence Berkeley National Laboratory, Berkeley, CA 94720, United States

∇ Center for Materials Crystallography at the Department of Chemistry and the Interdisciplinary Nanoscience Center, Aarhus University, Langelandsgade 140, 8000 Aarhus, Denmark

KEYWORDS: Nanoconfinement, Metal Hydrides, Metal-Organic Frameworks, Hydrogen Storage, Coordination Chemistry

ABSTRACT: A new form of hydride nanoconfinement is demonstrated through the creation of a molecular hydride species coordinated to binding sites inside the pores of a metal-organic framework (MOF). Magnesium borohydride, which has a high hydrogen capacity, is incorporated into the pores of UiO-67bpy ($Zr_6O_4(OH)_4(bpydc)_6$ with $bpydc^{2-}$ = 2,2'-bipyridine-5,5'-dicarboxylate) by solvent impregnation. The MOF retained its long-range order, and transmission electron microscopy and elemental mapping confirmed the retention of the crystal morphology and revealed a homogeneous distribution of the hydride within the MOF host. Notably, the B, N and Mg-edge XAS data confirm the coordination of Mg(II) to the N atoms of the chelating bipyridine groups. *In situ* ^{11}B MAS-NMR studies helped elucidate the reaction mechanism and revealed that complete hydrogen release from $Mg(BH_4)_2$ occurs as low as 200 °C. Sieverts and thermogravimetric measurements indicate an increase in the rate of hydrogen release, with the onset of hydrogen desorption as low as 120 °C, which is approximately 150 °C lower than that of the bulk material. Furthermore, density functional theory calculations support the improved dehydrogenation properties and confirm the drastically lower activation energy for B-H bond dissociation.

The controllable nanoconfinement of various guest species inside pores of micro- and mesoporous hosts has attracted significant research interest as the resulting composite materials not only exhibit the properties of both the host and the guest, but can also display unique and synergistic properties. Tuning the size, composition, and shape of nanoobjects encapsulated in porous hosts can enable the final composites to exhibit physical properties and reactivity very different from those of the separate constituents.[1-2] The properties of metal hydrides are particularly susceptible to changes when the particle size is reduced,[3-4] and nanoscaling has become one of the most promising strategies for improving the thermodynamics, kinetics, and reversibility.[5-6] Among the many synthetic approaches under consideration, confinement within nanoporous hosts offers a high level of synthetic control because of the ability to modify pore dimensions and chemical functionalities to control the properties of the hydride.[5,7] Porous carbon species,[8] carbon aerogels,[9] polymer matrices,[10] graphene,[11] carbon nanofibers,[12] and metal-organic frameworks (MOFs)[13] have all been used. These materials stabilize the nanocrystals or nanoclusters and inhibit their agglomeration. Notable achievements include reducing the heat of desorption by as much as 27 kJ mol^{-1} H_2,[14] lowering the H_2 release temperature by >150 °C,[15] stabilization of volatile metal borohydrides,[16] and complete elimination of the reaction steps responsible for the formation of thermodynamic sinks[17] and gas-phase impurities.[18]

Despite these successes, the limits of nanoscaling have never been fully understood. Addressing this gap in understanding is not only of fundamental scientific interest but is essential for determining whether nanoscaling is a viable approach to developing practical hydrogen storage materials. Currently, the limit of nanosizing using porous hosts is set by the accessible pore size. Carbon-based hosts such as carbon fibers, templated carbons, activated charcoals, and covalent-organic frameworks typically provide pore sizes between 1 and 10 nm.[19-21] Theoretical and experimental studies using such host materials show a marked increase in the dehydrogenation reaction rates of several hydrides when the particles are close to or below 1 nm.[22-23]

The smallest potentially achievable cluster size would be the immobilization of a single metal hydride molecule within a porous host. Even at a pore size of 1 nm, however, the immobilized hydride clusters contain many formula units and dozens of atoms. For example, we estimated that on average, the $NaAlH_4$ nanoclusters formed within Mg-MOF-74 (11.6 Å pores) contain eight formula units (48 atoms).[24] We therefore reasoned that chemical groups capable of charge transfer will be required to stabilize molecular-scale hydrides. Evidence supporting this hypothesis can be found in the work of

Majzoub *et al.*, who showed that incorporating heteroatoms affects the thermodynamics and the desorption pathway of the hydride, rendering the host material "noninnocent". Specifically, infiltrating N-doped porous carbons with $LiBH_4$ or $NaAlH_4$ altered the decomposition pathway and activation energy for hydrogen release.[25-26] In these studies, however, the as-synthesized hydride nanoparticles were far from the molecular limit, having sizes in the range of 1-10 nm depending on the pore size of the carbon species.

MOFs are an attractive alternative to other hosts because their pore size and chemical environment[27] are homogeneous and can be independently controlled within a crystalline (i.e., uniform) matrix. These materials consist of metal-containing secondary building units (SBUs) that are interconnected via multitopic organic linkers (e.g., carboxylates, pyridines, and imidazolates).[27] Due to their crystalline structure, theoretical property prediction is relatively straightforward.[28] MOFs have shown to be useful for the stabilization of hydride nanoparticles, substantially improving the H_2 release kinetics and thermodynamics.[29-31] For example, we successfully infiltrated $NaAlH_4$ within the nanopores of $Cu_3(btc)_2$ (btc^{3-} = 1,3,5-benzenetricarboxylate)[32] and $Mg_2(dobdc)$ ($dobdc^{4-}$ = 2,5-dioxido-1,4-benzenedicarboxylate).[24] Moreover, many MOFs possess functional groups capable of anchoring metal species through donor-acceptor type interactions between electron-rich donor atoms inside the porous host and electron-deficient metal centers.[33]

Here, we demonstrate a new molecular stabilization concept for nanoconfinement using UiO-67bpy (UiO = Universitetet i Oslo; $Zr_6O_4(OH)_4(bpydc)_6$ with $bpydc^{2-}$ = 2,2'-bipyridine-5,5'-dicarboxylate) as the 3D-porous framework. In this MOF, a $Zr_6O_4(OH)_4$ metal-oxo cluster is connected to 12 individual dicarboxylates, resulting in tetrahedral and octahedral pores with diameters of 11.5 Å and 23 Å, respectively.[34] The linkers of this MOF possess 2,2'-bipyridine sites that can coordinate metal cations.[35-38] We selected magnesium borohydride ($Mg(BH_4)_2$) for this investigation because it has one of the highest gravimetric hydrogen capacities (14.9 wt%). However, its practical application is hampered by sluggish kinetics and high desorption temperatures.[39-43] Previous studies show that Mg^{2+} readily forms stable five-membered ring chelate complexes with bipyridine.[44] In addition, the ammonia adduct, $(NH_3)_2Mg(BH_4)_2$, forms a tetrahedral complex, similar to the expected Mg coordination environment in a 2,2'-bipyridine-$Mg(BH_4)_2$ complex.[45] Interestingly, the desorption temperature of bulk $(NH_3)_2Mg(BH_4)_2$ is significantly lower than that of bulk $Mg(BH_4)_2$. In this work, we used solution impregnation[46] to introduce $Mg(BH_4)_2$ into the MOF pores to form $Mg(BH_4)_2$@UiO-67bpy (Figure 1). Using X-ray absorption spectroscopy (XAS), powder X-ray diffraction (PXRD), IR spectroscopy, N_2 porosimetry,

transmission electron microscopy (TEM) with energy dispersive X-ray (EDX) spectroscopy, and variable-temperature magic angle spinning-nuclear magnetic resonance spectroscopy (MAS–NMR), we established that $Mg(BH_4)_2$ molecules are coordinated to the $bpydc^{2-}$ linkers in the MOF. Sievert measurements coupled with thermogravimetric analysis (TGA) showed that the onset of hydrogen desorption from $Mg(BH_4)_2$@UiO-67bpy is >150 °C lower, and density functional theory (DFT) calculations predicted that the activation energy for the reaction is reduced by as much as 1.3 eV relative to that of the bulk material. Together, these results provide proof-of-concept that functionalized MOFs can act as suitable hosts for "molecular scaling" of metal hydrides and significantly alter their chemical reactivity.

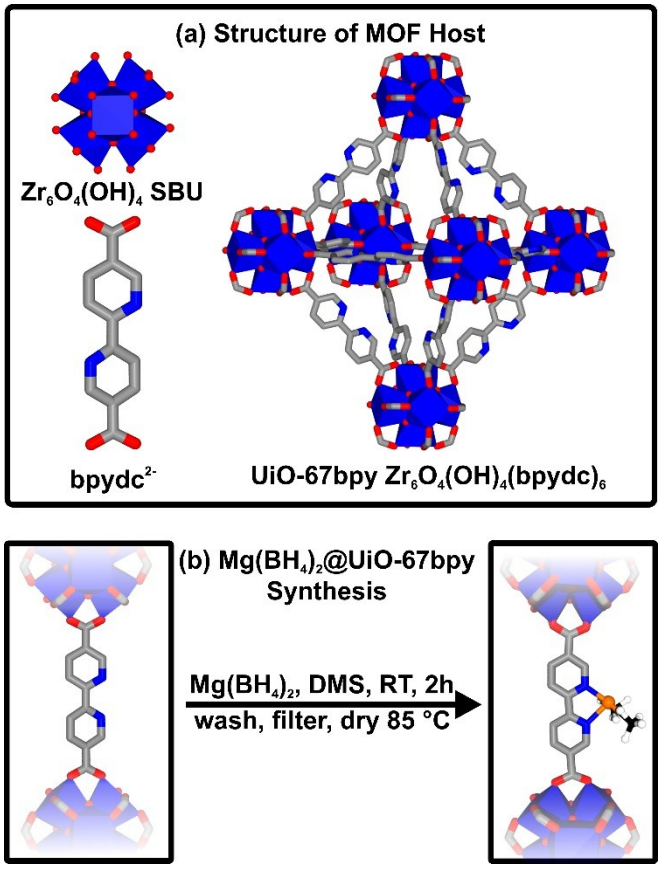

Figure 1: (a) Depiction of the organic and inorganic building blocks of the metal-organic framework UiO-67bpy and the octahedral pore. (b) Schematic of the installation of $Mg(BH_4)_2$ at the bipyridine sites of UiO-67bpy. For the sake of clarity, H atoms located on the organic linker have been omitted and only the *cis* isomer of 2,2'-bipyridine-5,5'-dicarboxylic acid is shown in panel (a). C, N, O, Mg, B and H are represented in grey, blue, red, orange, black and white, respectively. Blue polyhedrons represent the coordination environment of Zr.

RESULTS AND DISCUSSION

Synthesis and Structural Characterization

Magnesium borohydride was prepared by a slightly modified version of a literature synthesis (see the Methods Section for details).[47] UiO-67bpy was synthesized in accordance with the method published by Fei and Cohen on a larger scale.[48] $Mg(BH_4)_2$ was dissolved in dimethylsulfide (DMS), and the solution was added to a Schlenk tube containing UiO-67bpy. The suspension was stirred for 2 hours, and afterwards, the DMS solution was filtered off. The remaining solid was washed 3 times with dry, fresh DMS. The material was dried in vacuo overnight and stored under inert conditions in an argon-filled glovebox. A simplified depiction of the reaction procedure is shown in Figure 1b, and the potential bidentate κ_2-coordination of $Mg(BH_4)_2$ to the bipyridine unit in the cis conformation is highlighted. In addition, control experiments with unfunctionalized UiO-67 ($Zr_6O_4(OH)_4bpdc_6$; with $bpdc^{2-}$ = biphenyl-4,4'-dicarboxylic acid) have been performed (see Supporting Information for additional data).

The PXRD measurements and IR spectra (Figure 2a and b) show that the porous host material is still intact after exposure to $Mg(BH_4)_2$. However, the PXRD pattern suggests a substantial loss of crystallinity. No characteristic reflections for any of the common crystalline $Mg(BH_4)_2$ phases were present in the pattern, suggesting good dispersion within the host, without the formation of crystalline ordered domains that coherently scatter X-rays. The IR spectrum of $Mg(BH_4)_2$@UiO-67bpy showed stretches characteristic of carboxylates in the framework (1613 cm^{-1}, 1419 and 1385 cm^{-1}) and a broad signal indicating the presence of BH_4^- in the material (2200-2400 cm^{-1}). Furthermore, there is no indication of any sp^3 CH groups, indicating that DMS solvent was effectively removed during the activation process. Elemental analysis and inductively coupled plasma mass spectrometry (ICP-MS) suggested that the $Mg(BH_4)_2$ content is roughly two hydride formula units per bipyridine. N_2 sorption experiments (Figure 2c) were carried out at 77 K and were used to determine the pore volume and surface area of UiO-67bpy and $Mg(BH_4)_2$@UiO-67bpy. The total uptake at 1 bar was 601 cm^3g^{-1} for pristine UiO-67bpy and 10 cm^3g^{-1} for $Mg(BH_4)_2$@UiO-67bpy. The shape of the isotherm signalizes a low concentration of structural defects, as observed for other UiO-67 derivatives. The BET surface areas of UiO-67bpy and $Mg(BH_4)_2$@UiO-67bpy were 2108 $m^2\,g^{-1}$ and 23 $m^2\,g^{-1}$, respectively. The surface area of UiO-67bpy is in good agreement with the literature values.[48] The very low surface area of $Mg(BH_4)_2$@UiO-67bpy indicates that the pores are either completely filled with $Mg(BH_4)_2$ or that the pore entrances are blocked by the molecules, making the material inaccessible to nitrogen. Contrary, control experiments with the unfunctionalized analogue UiO-67 still showed substantial N_2 gas uptake

after treatment with $Mg(BH_4)_2$ solution, featuring a BET surface area of 923.7 m^2g-1 (compared to 2213.6 m^2g^{-1} for pristine UiO-67). These findings suggest a much lower loading of the material with $Mg(BH_4)_2$ and further manifest that the bipyridine groups are responsible for binding the $Mg(BH_4)_2$ within the UiO-67bpy framework (see Supporting Information for details).

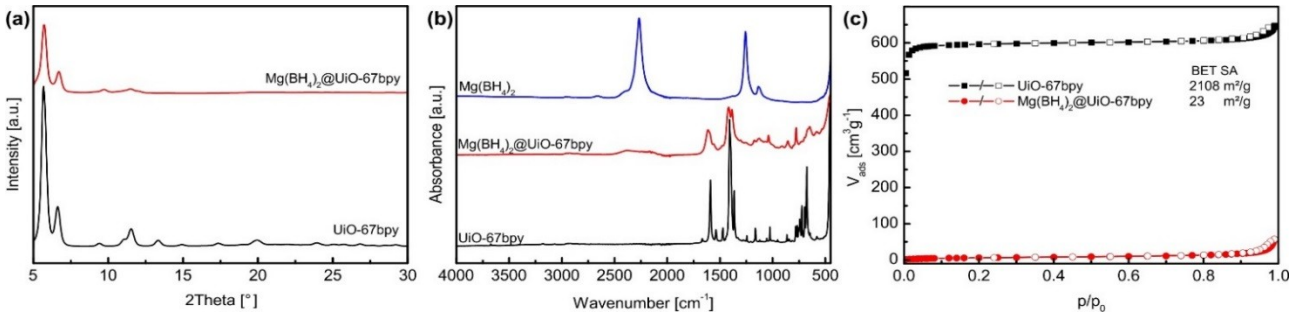

Figure 2: (a) Powder X-ray diffraction patterns of UiO-67bpy (black) and $Mg(BH_4)_2$@UiO-67bpy (red). (b) FTIR-spectra of $Mg(BH_4)_2$ (blue), $Mg(BH_4)_2$@UiO-67bpy (red) and UiO-67bpy (black). (c) N_2 sorption isotherms of UiO-67bpy (black squares) and $Mg(BH_4)_2$@UiO-67bpy (red circles). The filled and empty symbols represent the adsorption and desorption branches, respectively.

TEM micrographs and EDX elemental maps confirm the retention of the characteristic octahedral morphology of UiO-67bpy crystals and the homogeneous distribution of the hydride species throughout the sample after coordination of $Mg(BH_4)_2$ (Figure 3). The high angle annular darkfield (HAADF, Figure 3a) micrographs show octahedral crystallites ranging from 100-200 nm in size (for the micrographs of pristine UiO-67bpy, see Supporting Information Figure S8). Figure 3b-g show the elemental maps for zirconium, oxygen, carbon, nitrogen, magnesium and boron in $Mg(BH_4)_2$@UiO-67bpy (for further elemental maps and micrographs, see Supporting Information Figure S9). Additionally, the EDX spectra confirmed that no other elements were present as contaminants (i.e., sulfur from DMS or chlorine from $ZrCl_4$) in the sample (see Figures S10-S11).

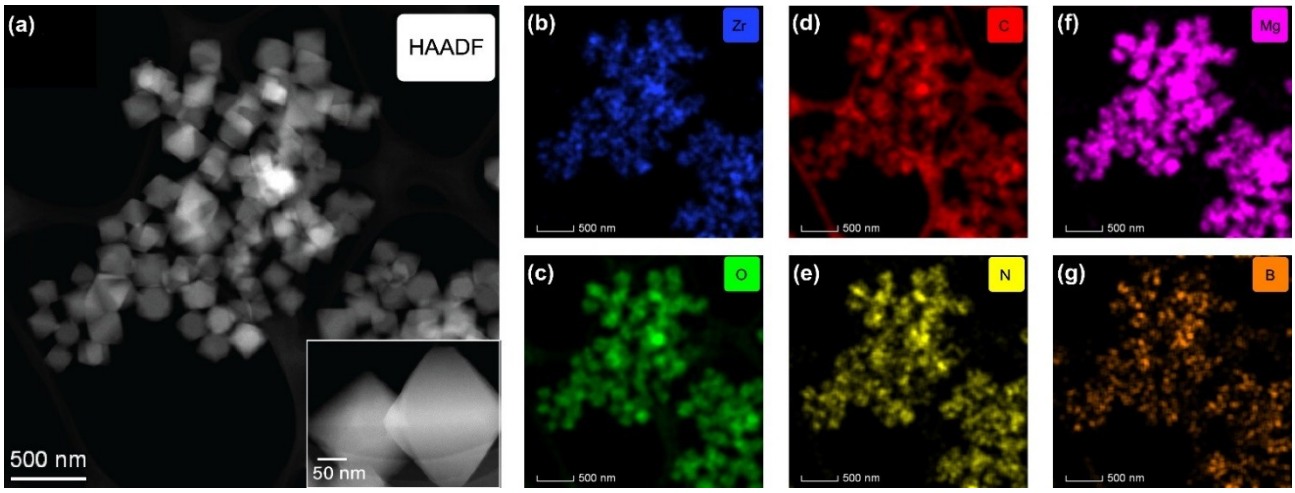

Figure 3: (a) High-angle annular darkfield TEM micrographs of a representative sample area of $Mg(BH_4)_2$@UiO-67bpy; the inset shows two octahedral crystals magnified further. EDX maps of the material showing zirconium (b), oxygen (c), carbon (d), nitrogen (e), magnesium (f) and boron (g).

The X-ray absorption spectra were acquired at beamline 8.0.1.4 at the Advanced Light Source at Lawrence Berkeley National Laboratory to probe the nature of $Mg(BH_4)_2$ inside the porous host and verify the coordination of $Mg(BH_4)_2$ to the bipyridine pockets. Figure 4 shows the measured N K-edge of the X-ray absorption spectra of UiO-67bpy before (Figure 4a) and after coordination to $Mg(BH_4)_2$. The edge position in the case of UiO-67bpy is located at 398.54 eV, whereas after coordination to $Mg(BH_4)_2$ is blueshifted to 398.85 eV. This shift to higher energy can be explained by charge transfer from the pyridyl nitrogens to Mg(II), increasing the binding energy of these electrons to the core.

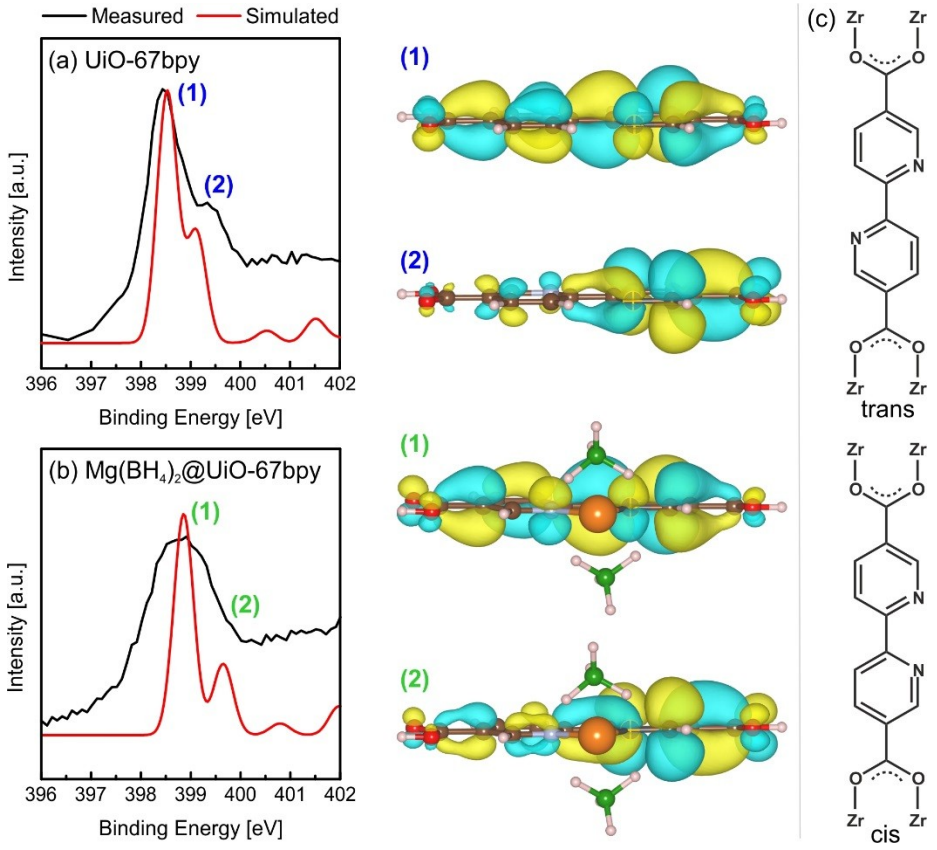

Figure 4: N K-edge X-ray absorption spectra of UiO-67bpy (a) and $Mg(BH_4)_2$@UiO-67bpy (b). The black graphs represent experimental results, and the red graphs are simulated spectra. The excited states are visualized by the charge densities on the right, and they show well defined π* features. (c) Schematic depiction of the cis and trans conformation of bipy in the structure of UiO-67bpy.

We obtained further insight into the nature of the hydride coordination to the MOF by modeling the interaction using DFT (Figure 4). Molecular H_2bpydc and $Mg(BH_4)_2$@H_2bpydc were used as models for calculating the spectra, and both the *cis* and *trans* conformations of the bipyridine were considered. For the gas-phase H_2bpydc molecule, the trans conformation (**1**) is 0.30 eV more stable than the cis conformation (**2**), as predicted by gas-phase DFT calculations at 0 K (Figure 4, top panel). When a

single $Mg(BH_4)_2$ monomer is coordinated to the nitrogen site, the cis conformation becomes more stable by 0.58 eV. Figures 4a and 4b show the simulated N K-edge spectra for the trans-H_2bpydc and cis-$Mg(BH_4)_2$@H_2bpydc structures, respectively. The first excited state at ~398.5 eV in Figure 4a (band 1) shows well-defined π^* features spread over the entire H_2bpydc molecule, whereas the second excited state, the shoulder at ~399.2 eV (band 2), is more localized near the excited atom. In the cis-$Mg(BH_4)_2$@H_2bpydc structure (Figure 4b), due to local interactions between the pyridinic N and Mg (band 2), the absorption at ~399.2 eV becomes more delocalized its intensity decreases. Notably, the simulated spectra of trans-H_2bpydc and cis-$Mg(BH_4)_2$@H_2bpydc ignore the effects of thermal fluctuations at room temperature. When thermal fluctuations are considered, we expect the spectra to broaden and the features will be less distinct, as is seen in the experimental spectra. Nevertheless, comparisons of the simulated and measured N K-edge spectra for UiO-67bpy and $Mg(BH_4)_2$@UiO-67bpy support our conclusion that $Mg(BH_4)_2$ species are coordinated to the pyridinic nitrogen in UiO-67bpy.

Hydrogen Desorption Properties of $Mg(BH_4)_2$@UiO-67bpy

To test the hypothesis that nanoconfinement and local environment influences the hydrogen desorption properties of $Mg(BH_4)_2$, we conducted TGA, RGA and Sieverts measurements, the results of which are displayed in Figure 5. The TGA trace of $Mg(BH_4)_2$@UiO-67bpy shown in Figure 6a suggests that the H_2 desorption onset temperature is indeed significantly lower than that of pristine $Mg(BH_4)_2$, with desorption beginning at ~120 °C compared to 270-280 °C for the pristine material. Moreover, the RGA-MS measurements indicate that the gas released from $Mg(BH_4)_2$@UiO-67bpy at low temperatures is primarily H_2, indicating no formation of B_2H_6 or decomposition products from the framework at low temperatures. At higher temperatures, decomposition products from the MOF (CO and CO_2, at m/z = 28 and 44, respectively) are released as well. We also performed Sieverts measurements on $Mg(BH_4)_2$@UiO-67bpy and found that the material released 0.22 wt% H_2 at 150 °C, which again is significantly lower than the initial hydrogen released from bulk $Mg(BH_4)_2$. This amount translates to approximately 1 wt% H_2 based on normalization to $Mg(BH_4)_2$ according to the formula $(Mg(BH_4)_2)_{12}$@UiO-67bpy (derived from elemental analysis, which suggested two $Mg(BH_4)_2$ per linker, see the Methods Section). The amount of released hydrogen determined by the Sieverts method contains some uncertainty due to the low loading of active species (i.e., 150 mg of $(Mg(BH_4)_2)_{12}$@UiO-67bpy, which only contains approximately 35 mg of hydride), and it is typically lower compared to other nanoconfined magnesium borohydride systems (section S8 in SI).

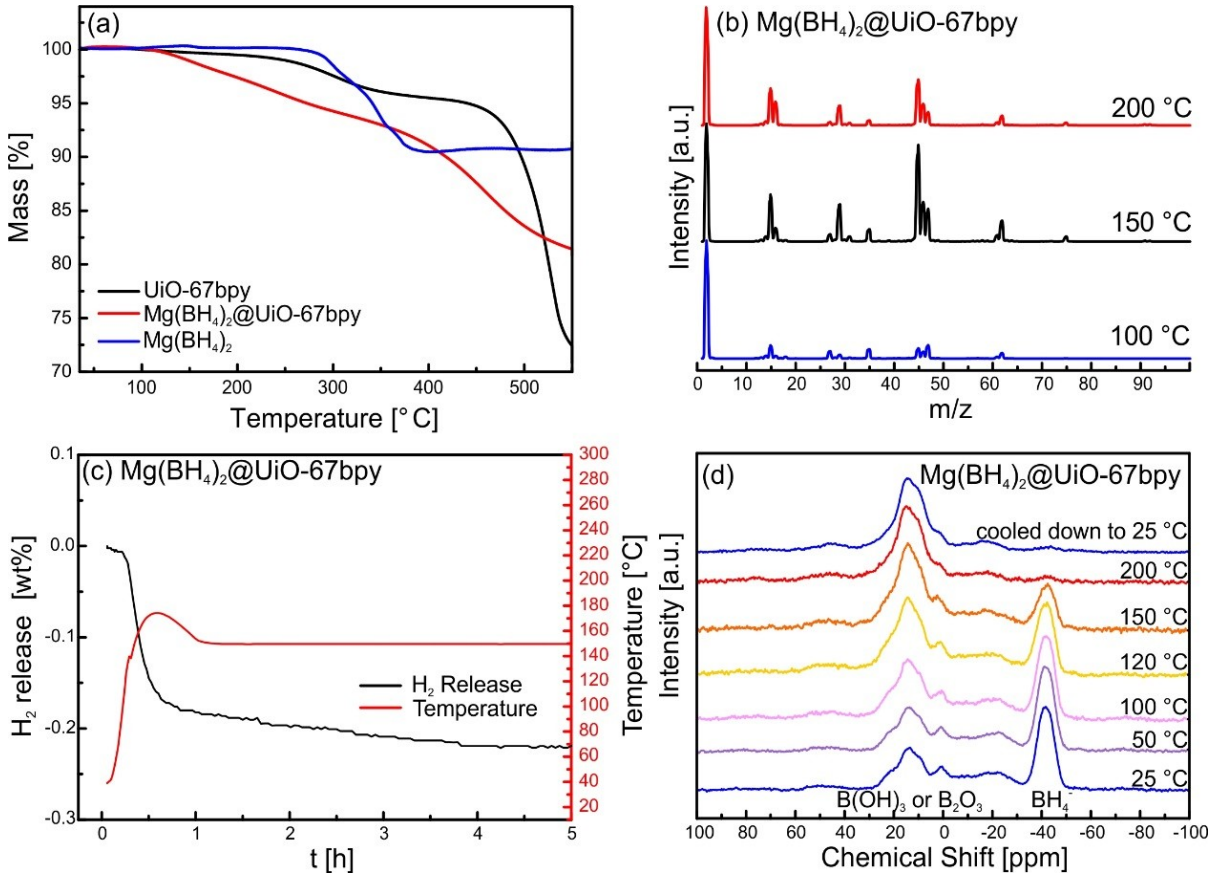

Figure 5: (a) TGA measurements of UiO-67bpy (black), $Mg(BH_4)_2$@UiO-67bpy (red) and $Mg(BH_4)_2$ (blue). (b) Analysis of the composition of the gas released from $Mg(BH_4)_2$@UiO-67bpy at 100 °C, 150 °C and 200°C determined using a residual gas analyzer mass spectrometer. (c) Sieverts measurement of $Mg(BH_4)_2$@UiO-67bpy to quantify the amount of gas released at 150 °C. The red curve represents the temperature profile, and the black curve represented the wt% of released hydrogen. (a) Variable temperature ^{11}B-MAS NMR of $Mg(BH_4)_2$@UiO-67bpy.

The structural integrity of the material following dehydrogenation was evaluated using XRD and IR spectroscopy (see the Supporting Information). The spectra of the MOF still showed some of its characteristic diffraction peaks; however, their intensities were significantly decreased, and the obtained IR spectra was lacking most of the characteristic signals for the hydride and MOF. Attempts to rehydrogenate the material under mild conditions (140 bar H_2, 150-200 °C) were unsuccessful, and the intensities in the resulting XRD patterns and IR spectra were negligible, suggesting complete decomposition of the material (see Supporting Information Figures S6 and S7). It is possible that higher hydrogen pressures are required to regenerate the material. For instance, $Mg(BH_4)_2$ was shown to be fully reversible only at 390-400 °C and 900-1000 bar H_2,[49] which is well-beyond the stability of the UiO-67bpy framework.

^{11}B variable-temperature MAS-NMR was used to further probe the reaction pathway and analyze the nature of the $Mg(BH_4)_2$ inside the pore space. Interestingly, even at room temperature, other species in addition to BH_4^- anions were observed. The BH_4^- species shows a signal at -41.1 ppm. A minor fraction of the material was present as a BX_3 species, most likely BH_3 or B_2H_6 encapsulated within the composite (signal at 0.5 ppm). Last, a broad and relatively intense signal centered at approximately 14.1 ppm was present, and this signal can be assigned to B-O species. We attribute these signals to the reactive boron atoms that bind to MOF oxygen atoms upon hydrogen release. The formation of oxide layers around the Lewis-acidic Zr SBUs is not unprecedented and has been reported in several other studies.[50] The formation of such stable B-O species may also be responsible for the lack of reversible hydrogen uptake from the desorbed version of the $Mg(BH_4)_2$@UiO-67bpy material. Furthermore, the determined $Mg(BH_4)_2$ content of the samples, which exceeds full occupation of the chelating sites of the bipyridine, can be explained by coordination/reaction of additional $Mg(BH_4)_2$ at the Zr-Oxo Clusters. During variable-temperature NMR experiments, a continuous decrease in the content of BH_4^- in the material with increasing temperature was observed (Figure 5d). Between 150 °C and 200 °C, all the hydride was consumed. However, the amount of boron-containing oxide or hydroxide species increased during the heating process until all the boron was present in this form. Remarkably, the spectra confirm that unlike in bulk $Mg(BH_4)_2$, no $[B_{10}H_{10}]^{2-}$ or $[B_{12}H_{12}]^{2-}$ clusters form upon heating (Figure 5d). In addition, the formation of such large *closo*-borate clusters would require significant reorganization of the framework, as both the $[B_{10}H_{10}]^{2-}$ or $[B_{12}H_{12}]^{2-}$ anions are larger than the UiO-67bpy pore size. *Ex situ* XAS measurements further confirm this observation (see Supporting Information Figures S12-S14).

Theoretical Calculations and Mechanistic Insights

From the N K-edge XAS and ^{11}B NMR chacterization, it is observed that $Mg(BH_4)_2$ interact directly with the bipyridine pocket on the $bpydc^{2-}$ linker and the oxygen atoms from the $Zr_6O_4(OH)_4$ metal clusters. These $Mg(BH_4)_2$-N and $Mg(BH_4)_2$-O interactions can influence the B-H bonding strength in the BH_4^- unit due to charge relocalization and thereby affect its hydrogen release kinetics. Here we use the climbing image nudged elastic band (NEB) method to estimate and compare the relative B-H bonding strength in bulk γ-$Mg(BH_4)_2$ and $Mg(BH_4)_2$@UiO-67bpy. As shown in Figure 6(a), the activation energies for B-H bond dissociation are calculated for bulk γ-$Mg(BH_4)_2$ (black) and single $Mg(BH_4)_2$ molecules adsorbed in UiO-67bpy at both N-site (blue) and O-site (red). The reaction path for the NEB calculation of bulk γ-$Mg(BH_4)_2$ was defined as the concerted removal of two H atoms from neighboring BH_4 units (one from each BH_4^-) to form a H_2 molecule (Figure 6(b)). The associated activation energy for this process is about 4.8 eV for bulk γ-$Mg(BH_4)_2$, which is lowered to 3.5 eV for a $Mg(BH_4)_2$

monomer chelated by nitrogen atoms. This likely represents the lower bound for the B-H dissociation energy of $Mg(BH_4)_2$ adsorbed at the N-site in UiO-67bpy, as it is conceivable that $Mg(BH_4)_2$ nanoagglomerates consisting of a few molecules forms inside UiO-67bpy. This is in accordance with the elemental analysis and ICP-MS results, which suggest a $Mg(BH_4)_2$:bipy ratio of 2:1. For comparison, a model was derived with pores completely filled with $Mg(BH_4)_2$ to estimate the NEB-based activation energy for the other extreme. As shown in Figure S15, the NEB-based activation energies for B-H dissociation in selected N-Mg-BH_4 coordination environments in $Mg(BH_4)_2$@UiO-67bpy are higher than those in the monomer case but remained at least 0.5 eV lower than those of ibulk.

To examine the effect of O-coordination of $Mg(BH_4)_2$ to UiO-67bpy, we first computed the $Mg(BH_4)_2$ adsorption energies at the O-sites. In Figure 6(c), we present the lowest energy (-0.806 eV) configuration for a single $Mg(BH_4)_2$ molecule adsorbed at the O-sites, from which Mg-O interaction is observed as well as BH_4-OH interaction (highlighted in orange in Figure 6(c)). Intuitively, we expect that this BH_4-OH, essentially the H^--H^+ interaction can promote H_2 release. As shown by the red curve in Figure 6(a), the activation energy for H_2 release from direct BH_4-OH interaction is approximately 2.5 eV, which is much lower than that in bulk γ-$Mg(BH_4)_2$. In the SI, we discuss another H_2 release pathway at the O-site that involves multiple steps and is mediated by the H^--OH interaction. Overall, the calculations support the notion that both bipyridine and oxygen coordination environments can improve the initial dehydrogenation kinetics of $Mg(BH_4)_2$.

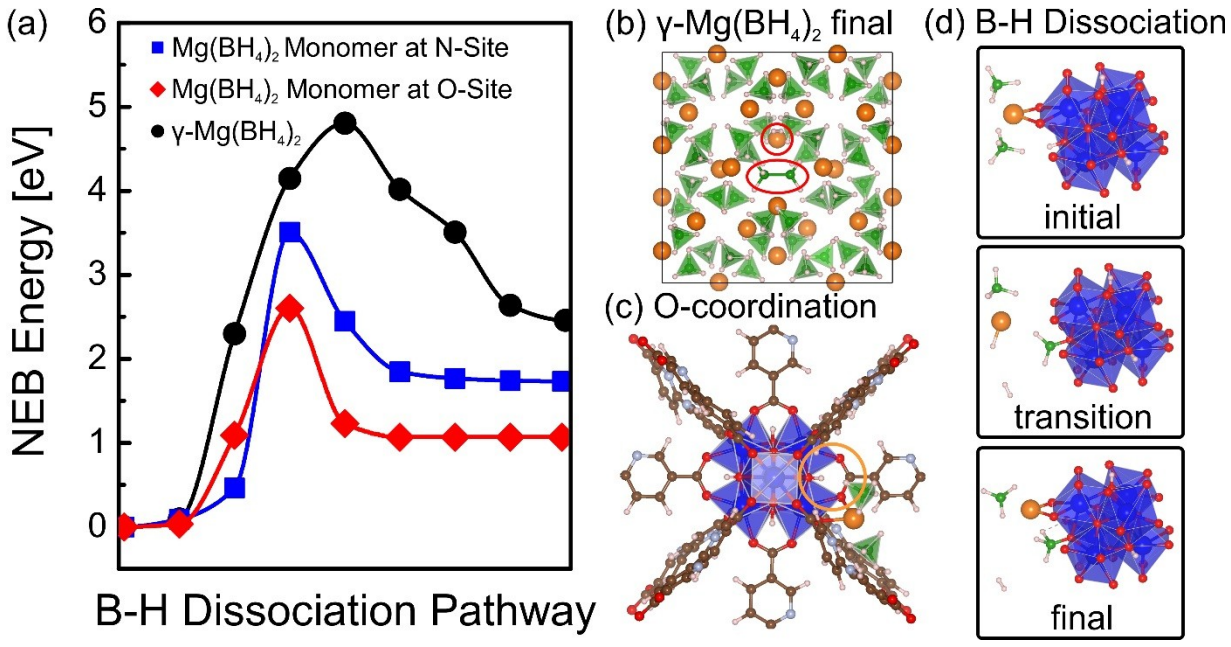

Figure 6: (a) Calculated activation energies for B-H dissociation in γ-$Mg(BH_4)_2$ and $Mg(BH_4)_2$ adsorbed in UiO-67bpy. (b) Final state along the NEB reaction pathway of γ-$Mg(BH_4)_2$ after H_2 release. (c) Lowest

energy configuration for a single $Mg(BH_4)_2$ molecule adsorbed at the O-site in UiO-67bpy. (d) Initial, transition and final state structure representations for B-H dissociation of $Mg(BH_4)_2$ adsorbed at the O-site. For clarity, only the $Mg(BH_4)_2$ molecule and the $Zr_6O_4(OH)_4$ center are shown in these structure representations. The hydrogen, carbon, oxygen, nitrogen and magnesium atoms are represented in pink, brown, red, blue and orange, respectively. The blue polyhedra represent the $Zr_6O_4(OH)_4$ unit in UiO-67bpy and the green polyhedra represent the BH_4 anions in $Mg(BH_4)_2$.

CONCLUSIONS

We present here a conceptually new strategy for nanoscaling metal hydrides by anchoring metal ions to electron-rich chelating groups of a MOF host. We use magnesium borohydride confined in UiO-67bpy as a case study to probe the limit of nanoconfinement of metal hydrides. Our TEM/EDX measurements show that the $Mg(BH_4)_2$ species are evenly distributed throughout the UiO-67bpy crystals upon liquid-phase infiltration, with no large agglomerates present. These results, coupled with the XAS measurements and DFT calculations support the conclusion that an extreme case of nanoconfinement is achieved in this system, and metal hydride species exist as molecular species, rather than large agglomerates or nanoparticles. The use of a MOF host to confine hydrogen storage materials may seem counterintuitive, as the molecular movement of the reacting species could be restricted by the presence of pore walls. In reality, our modeling and experiments suggest that the reaction rates are accelerated by the confinement, as evidenced by the weakening the B-H bonds and the lowering of the activation energies for B-H dissociation compared to bulk $Mg(BH_4)_2$. The next step in the development of these molecularly dispersed hydride systems is to use lightweight hosts that do not contain heavy Zr atoms and eliminate oxygen atoms from the secondary building units of the MOFs to prevent stable B-O bond formation known to limit reversibility. This strategy could also prevent the formation of undesirable intermediates, such as $[B_{12}H_{12}]^{2-}$[51] and $[B_{10}H_{10}]^{2-}$[52] *closo*-borates upon thermal decomposition, as these anions are simply too large to form inside the MOF pores. Nevertheless, this proof-of-concept study offers a clear path towards molecularly confined hydrogen storage materials and reactions.

These results support the concept of “molecularly dispersed” metal hydrides and indicate that this strategy could become an important tool for altering and controlling both the kinetics and thermodynamics of hydrogen storage processes. MOFs, organic polymers,[53] conjugated microporous polymers[54] or covalent-organic frameworks[55] could all serve as suitable hosts due to their small pore sizes and potential for functionalization with various chemical groups to facilitate the binding of metal hydride species. The synthetic strategy we introduced here could enable the precise control of the

orientation of the hydrogen atoms on surfaces, for example, by creating favorable hydridic-protic H···H interactions.[5] Finally, strict control over the orientation of hydrides at the nanoscale can enable precise placement of hydrogen atoms in the vicinity of catalytic centers to further accelerate the rate of H_2 storage processes and potentially enable reversible hydrogen uptake and release. More broadly, we envision a wide range of uses for "molecularly dispersed" metal hydrides to address important problems within the areas of emerging nanoscale materials for energy generation and storage.

METHODS

Synthesis of Magnesium Borohydride

$Mg(BH_4)_2$ was synthesized using a slightly modified version of a literature procedure.[47] A dry Schlenk flask was equipped with a stirring bar, heated in vacuo, flushed several times with argon as a protecting gas and filled with dry toluene (150 mL) obtained from a solvent purification system (Innovation Technology PureSolv). Neat $BH_3{\cdot}SMe_2$ (350 mmol, 35 mL) was added via syringe, and the mixture was stirred for 10 min. The Schlenk tube was equipped with a preheated and argon-flushed pressure-equalizing dropping funnel, and the dropping funnel was filled with 100 mL of 1 M $Mg(Bu)_2$ (100 mmol). The $Mg(Bu)_2$ was added dropwise to the reaction mixture over 30 min, upon which a white precipitate formed. The reaction mixture is then stirred overnight. Subsequently, the mixture was left to settle, and the supernatant was removed via cannula. Fresh, dry toluene was added, and the mixture was stirred for 15 min. The toluene was replaced a total of three times. Afterwards, the majority of the supernatant was removed via cannula, and the remainder was condensed into a cooling trap. The white $Mg(BH_4)_2$ powder was heated under vacuum overnight at 85 °C. The purity of the solid was confirmed by PXRD and IR spectroscopy. The as prepared magnesium borohydride was stored in an argon-filled glovebox. Yield: 4.8 g.

Synthesis of UiO-67bpy

The MOF was prepared in accordance with a known literature procedure.[48] A stock solution of the reactants was prepared by dissolving $ZrCl_4$ (3.15 mmol, 735 mg), H_2bpydc (3.15 mmol, 780 mg) and glacial acetic acid (94.5 mmol, 5.4 mL) in DMF. The mixture was sonicated and then divided into 4-mL portions in 30 individual DRAM vials (22 mL). The vials were placed in an oven at 120 °C for 24 h. After the reaction, the vials were cooled down, and all the batches were pooled into centrifuge tubes. The material was washed three times with dichloromethane and sonicated. Afterwards, the material was

filtered, transferred to a Schlenk flask and dried in vacuo at 180 °C overnight. The material was stored in an argon-filled glovebox until further use. Yield: 920 mg.

Synthesis of $Mg(BH_4)_2$@UiO-67bpy

$Mg(BH_4)_2$ (200 mg 3.7 mmol) was placed in a Schlenk flask, and dimethylsulfide (DMS, dried over 3 Å molecular sieves for three days) (~20 mL) was added until all the solid was dissolved. Afterwards, the dried MOF material (500 mg, 0.2 mmol) was added to the reaction mixture. The MOF suspension in the $Mg(BH_4)_2$ solution was stirred for 2 h until a marked color change to orange-brown was observed (note that this color change was not observed in the analogous experiment with the parent UiO-67 species with 3,3'-biphenyldicarboxylic acid, without the bipyridine moieties, see the Supporting Information for details). The DMS was then removed via cannula, and the reaction product was washed three times with 20 mL of fresh, dry DMS. Afterwards, the material was dried at 85 °C overnight. Elemental analysis (CHNS Analysis) (% theoretical values based on $(Mg(BH_4)_2)_{12}@Zr_6O_4(OH)_4(bpydc)_6$) C: 29.15 (found) 31.10 (theor.); H: 4.28 (found) 4.93 (theor.); N: 6.65 (found) 6.05 (theor.); Zr(ICP-MS): 18.71 (found) 19.69 (theor.); Mg(ICP-MS): 9.85 (found) 10.49 (theor.)

Characterization

Powder X-ray diffraction patterns were acquired on an Oxford Diffraction Supernova in capillary mode using CuKα radiation. Measurements were recorded using a CCD detector at 77 mm from the samples with an exposure time of 60 s at 4 different positions. The recorded 2D images were added and integrated to generate a 1D pattern. The samples were packed into quartz capillaries inside a glovebox and sealed with wax. *Infrared Spectra* were collected on an Agilent Technologies Cary-630 instrument equipped with an ATR unit located in a glovebox. Before each measurement, a background spectrum was collected. *Nitrogen physisorption isotherms* were measured on a Micromeritics ASAP 2020 porosimeter at 77 K using a N_2 bath for cooling. Prior to each measurement, 50-100 mg of sample was degassed in vacuo overnight. All gases used for the measurements were 99.999 % purity or higher. *Transmission electron microscopy and energy dispersive X-ray spectroscopy elemental mapping* were conducted on a ThermoFisher Titan Themis Z TEM operated at 300 kV. The samples were immersed in dry toluene and then dropcast onto Cu grids coated with a lacey carbon film. EDX data were collected with a Super-X four-quadrant silicon drift detector (SDD) with a collection solid angle of approximately 0.7 sr. Data were collected with pixel times of 10-20 µs, and multiple frames were collected with drift correction for total acquisition times of approximately 10 min. Elemental maps were generated after

parabolic background subtraction. *X-ray absorption spectra* were acquired at Beamline 8.0.1.4 at the Advanced Light Source. The beamline energy resolutions are approximately 0.1 eV for the B K-edge, 0.2 eV for the N K-edge, and 0.8 eV for the Mg K-edge spectra. All samples were prepared in an Ar-filled glovebox (H_2O, O_2 <0.1 ppm) with an UHV compatible transfer tool, allowing the samples to be mounted in the experimental chamber without ever exposing them to air. XAS measurements were carried out under UHV conditions at less than $1.0x10^{-9}$ torr. XAS was conducted in surface-sensitive total electron yield mode and bulk sensitive fluorescence mode. Energy calibrations were performed using B_2O_3, *h*-BN and MgO as references. *Elemental analyses* were conducted in the microanalytical laboratories at Galbraith Laboratories, Knoxville, TN. *Inductively plasma coupled mass spectrometry* measurements were performed at ALS Environmental, Inc. *Thermogravimetric* analyses were performed using a Mettler-Toledo TGA/DSC 1 STARe. Inside a glovebox, 2-5 mg samples were transferred to pre-weighed aluminum crucibles. The crucibles were equipped with pre-weighed aluminum lids and sealed with a hydraulic press to make the system airtight. The lid was pierced in the instrument under protective gas flow. The samples were heated with a ramp of 5 K min^{-1} under an argon flow of 20 ccm min^{-1}. *Gas analysis* was performed using a custom-built set-up equipped with a turbo molecular pump (Agilent V70D) and a Stanford Research Systems CIS 200 closed ion source mass spectrometer with a sample range from 1-200 atomic mass units. The samples were prepared inside a glovebox in a home-built reactor that was heated with a heating mantle. *Sieverts measurements* were performed on a PCT-Pro2000 instrument by Setaram. Approximately 150 mg of sample was transferred to the reactor connected to the instrument. Prior to each measurement, the reactor was evacuated, and the volume was calibrated. The reactor was heated in an isothermal furnace connected to the Sieverts instrument. *Solid-state NMR spectroscopy* experiments were performed at 11.7 T (500.18 MHz for ^{1}H and 160.48 MHz for ^{11}B) on an Agilent VNMRS spectrometer at the Environmental Molecular Sciences Laboratory (EMSL), Pacific Northwest National Laboratory (PNNL), using a home-built 5-mm MAS probe double tuned to $^{1}H/^{11}B$. The rotors were CAVERN-style zirconia sleeves (Revolution NMR that were modified to accommodate a double O-ring and a Vespel bushing to seal the sample up to 225 bar at 250 °C) that have been previously described.[56] Chemical shifts were referenced to 1 M boric acid (aq.) at 19.2 ppm, and nonselective $\pi/2$ pulses were calibrated as 5.2 μs on the same sample. Borohydride samples were packed into the rotors in a glovebox under an inert nitrogen atmosphere and sealed with the O-ring seals mentioned above. For quantitative direct polarization (DP) experiments, the rf pulse was reduced to a selective $\pi/20$ or 0.26 μs. The recycle delays were 1 s. The ^{1}H decoupling scheme was SPINAL-16[57] with a field strength of approximately 42 kHz.

Theoretical Calculations

DFT calculations using VASP were performed to obtain the optimized structures of the H_2bpydc backbone, $Mg(BH_4)_2$@H_2bpydc and $Mg(BH_4)_2$@UiO-67bpy. PAW pseudopotentials with a kinetic cutoff of 600 eV were used in the VASP calculations. XAS calculations were performed within the excited core-hole approximation using the Quantum ESPRESSO code package.[58-59] A modified ultrasoft pseudopotential with a core electron removed from the 1s state was used to model the N K-edge excitation, and a sufficiently large supercell with gamma point sampling was used to ensure that the excited state did not interact with its image under the periodic boundary conditions. All the DFT calculations performed in this work used the PBE-GGA exchange-correlation functional. To obtain a smooth and continuous XAS spectrum, the calculated transition probabilities at each energy were convoluted using a Gaussian broadening of 0.2 eV. A previously established alignment scheme was used to shift all the calculated N K-edge spectra using molecular N_2 as a reference. The climbing image nudged elastic band (NEB) method was used to approximate the B-H bonding strength or dissociation energy.

ASSOCIATED CONTENT

Supporting Information. Control experiments with $Mg(BH_4)_2$@UiO-67 and additional TEM micrographs, EDX spectra, XAS data and DFT calculations. This material is available free of charge via the Internet at http://pubs.acs.org.

AUTHOR INFORMATION

Corresponding Authors

Mark D. Allendorf (mdallen@sandia.gov); Vitalie Stavila (vnstavi@sandia.gov).

Author Contributions

The manuscript was written through contributions of all authors. All authors have given approval to the final version of the manuscript.

ACKNOWLEDGMENTS

AS gratefully acknowledges the German Research Foundation (DFG) for a postdoctoral fellowship (SCHN 1539/1-1). Sandia National Laboratories is a multimission laboratory managed and operated by National Technology and Engineering Solutions of Sandia, LLC., a wholly owned subsidiary of Honeywell International, Inc., for the U.S. Department of Energy's National Nuclear Security

Administration under contract DE-NA-0003525. The authors gratefully acknowledge funding from the U.S. Department of Energy, Office of Energy Efficiency and Renewable Energy, Fuel Cell Technologies Office, through the Hydrogen Storage Materials Advanced Research Consortium (HyMARC). The computational portion of the work was performed under the auspices of the DOE by Lawrence Livermore National Laboratory (LLNL) under Contract DE-AC52-07NA27344, with computing support from the LLNL Institutional Computing Grand Challenge program. This work was supported by the Laboratory Directed Research and Development (LDRD) program at Sandia National Laboratories. This research used resources from the Advanced Light Source, which is a DOE Office of Science User Facility under contract no. DE-AC02-05CH11231. The work was also supported by the Danish National Research Foundation, Center for Materials Crystallography (DNRF93) and the Danish Council for Independent Research, Technology and Production (HyNanoBorN, DFF – 4181-00462). A portion of the research was performed using the Environmental Molecular Sciences Laboratory (grid.436923.9), a DOE Office of Science User Facility sponsored by the Office of Biological and Environmental Research, located at the Pacific Northwest National Laboratory (PNNL). PNNL is operated by Battelle for the DOE under contract DE-AC05- 76RL0 1830. This paper describes objective technical results and analysis. Any subjective views or opinions that might be expressed in the paper do not necessarily represent the views of the U.S. Department of Energy or the United States Government.

References

1. Chen, L.; Luque, R.; Li, Y., Controllable design of tunable nanostructures inside metal–organic frameworks. *Chemical Society Reviews* **2017,** *46* (15), 4614-4630.
2. Seo, M.; Chung, T. D., Nanoconfinement effects in electrochemical reactions. *Current Opinion in Electrochemistry* **2019,** *13*, 47-54.
3. He, T.; Cao, H.; Chen, P., Complex Hydrides for Energy Storage, Conversion, and Utilization. *n/a* (n/a), 1902757.
4. Paskevicius, M.; Jepsen, L. H.; Schouwink, P.; Černý, R.; Ravnsbæk, D. B.; Filinchuk, Y.; Dornheim, M.; Besenbacher, F.; Jensen, T. R., Metal borohydrides and derivatives – synthesis, structure and properties. *Chemical Society Reviews* **2017,** *46* (5), 1565-1634.
5. Schneemann, A.; White, J. L.; Kang, S.; Jeong, S.; Wan, L. F.; Cho, E. S.; Heo, T. W.; Prendergast, D.; Urban, J. J.; Wood, B. C.; Allendorf, M. D.; Stavila, V., Nanostructured Metal Hydrides for Hydrogen Storage. *Chemical Reviews* **2018,** *118* (22), 10775-10839.
6. Yu, X. B.; Tang, Z. W.; Sun, D. L.; Ouyang, L. Z.; Zhu, M., Recent advances and remaining challenges of nanostructured materials for hydrogen storage applications. *Progress in Materials Science* **2017,** *88*, 1-48.
7. Nielsen, T. K.; Besenbacher, F.; Jensen, T. R., Nanoconfined hydrides for energy storage. *Nanoscale* **2011,** *3* (5), 2086-2098.
8. Ngene, P.; van den Berg, R.; Verkuijlen, M. H. W.; de Jong, K. P.; de Jongh, P. E., Reversibility of the hydrogen desorption from NaBH4 by confinement in nanoporous carbon. *Energy & Environmental Science* **2011,** *4* (10), 4108-4115.
9. Nielsen, T. K.; Manickam, K.; Hirscher, M.; Besenbacher, F.; Jensen, T. R., Confinement of MgH2 Nanoclusters within Nanoporous Aerogel Scaffold Materials. *ACS Nano* **2009,** *3* (11), 3521-3528.

10. Jeon, K.-J.; Moon, H. R.; Ruminski, A. M.; Jiang, B.; Kisielowski, C.; Bardhan, R.; Urban, J. J., Air-stable magnesium nanocomposites provide rapid and high-capacity hydrogen storage without using heavy-metal catalysts. *Nature Materials* **2011,** *10*, 286.
11. Cho, E. S.; Ruminski, A. M.; Aloni, S.; Liu, Y.-S.; Guo, J.; Urban, J. J., Graphene oxide/metal nanocrystal multilaminates as the atomic limit for safe and selective hydrogen storage. *Nature Communications* **2016,** *7*, 10804.
12. Baldé, C. P.; Hereijgers, B. P. C.; Bitter, J. H.; de Jong, K. P., Facilitated Hydrogen Storage in NaAlH4 Supported on Carbon Nanofibers. *Angewandte Chemie International Edition* **2006,** *45* (21), 3501-3503.
13. Rossin, A.; Tuci, G.; Luconi, L.; Giambastiani, G., Metal-Organic Frameworks as Heterogeneous Catalysts in Hydrogen Production from Lightweight Inorganic Hydrides. *Acs Catalysis* **2017,** *7* (8), 5035-5045.
14. Zhang, Y.; Zhang, W.-S.; Wang, A.-Q.; Li-Xian, S.; Fan, M.-Q.; Chu, H.-L.; Sun, J.-C.; Zhang, T., LiBH4 nanoparticles supported by disordered mesoporous carbon: Hydrogen storage performances and destabilization mechanisms. *International Journal of Hydrogen Energy* **2007,** *32* (16), 3976-3980.
15. Ngene, P.; van Zwienen, M.; de Jongh, P. E., Reversibility of the hydrogen desorption from LiBH4: a synergetic effect of nanoconfinement and Ni addition. *Chemical Communications* **2010,** *46* (43), 8201-8203.
16. Callini, E.; Szilágyi, P. Á.; Paskevicius, M.; Stadie, N. P.; Réhault, J.; Buckley, C. E.; Borgschulte, A.; Züttel, A., Stabilization of volatile Ti(BH4)3 by nano-confinement in a metal–organic framework. *Chemical Science* **2016,** *7* (1), 666-672.
17. Wood, B. C.; Stavila, V.; Poonyayant, N.; Heo, T. W.; Ray, K. G.; Klebanoff, L. E.; Udovic, T. J.; Lee, J. R. I.; Angboonpong, N.; Sugar, J. D.; Pakawatpanurut, P., Nanointerface-Driven Reversible Hydrogen Storage in the Nanoconfined Li–N–H System. *Advanced Materials Interfaces* **2017,** *4* (3), 1600803.
18. Zhang, H. Y.; Xia, G. L.; Zhang, J.; Sun, D. L.; Guo, Z. P.; Yu, X. B., Graphene-Tailored Thermodynamics and Kinetics to Fabricate Metal Borohydride Nanoparticles with High Purity and Enhanced Reversibility. *Advanced Energy Materials* **2018,** *8* (13).
19. Zlotea, C.; Cuevas, F.; Paul-Boncour, V.; Leroy, E.; Dibandjo, P.; Gadiou, R.; Vix-Guterl, C.; Latroche, M., Size-Dependent Hydrogen Sorption in Ultrasmall Pd Clusters Embedded in a Mesoporous Carbon Template. *Journal of the American Chemical Society* **2010,** *132* (22), 7720-7729.
20. Kalidindi, S. B.; Oh, H.; Hirscher, M.; Esken, D.; Wiktor, C.; Turner, S.; Van Tendeloo, G.; Fischer, R. A., Metal@COFs: Covalent Organic Frameworks as Templates for Pd Nanoparticles and Hydrogen Storage Properties of Pd@COF-102 Hybrid Material. *Chemistry – A European Journal* **2012,** *18* (35), 10848-10856.
21. Zhao-Karger, Z.; Hu, J.; Roth, A.; Wang, D.; Kübel, C.; Lohstroh, W.; Fichtner, M., Altered thermodynamic and kinetic properties of MgH2 infiltrated in microporous scaffold. *Chemical Communications* **2010,** *46* (44), 8353-8355.
22. Wagemans, R. W. P.; van Lenthe, J. H.; de Jongh, P. E.; van Dillen, A. J.; de Jong, K. P., Hydrogen Storage in Magnesium Clusters: Quantum Chemical Study. *Journal of the American Chemical Society* **2005,** *127* (47), 16675-16680.
23. Yamauchi, M.; Ikeda, R.; Kitagawa, H.; Takata, M., Nanosize Effects on Hydrogen Storage in Palladium. *The Journal of Physical Chemistry C* **2008,** *112* (9), 3294-3299.
24. Stavila, V.; Bhakta, R. K.; Alam, T. M.; Majzoub, E. H.; Allendorf, M. D., Reversible Hydrogen Storage by NaAlH4 Confined within a Titanium-Functionalized MOF-74(Mg) Nanoreactor. *Acs Nano* **2012,** *6* (11), 9807-9817.
25. Carr, C. L.; Jayawardana, W.; Zou, H.; White, J. L.; El Gabaly, F.; Conradi, M. S.; Stavila, V.; Allendorf, M. D.; Majzoub, E. H., Anomalous H2 Desorption Rate of NaAlH4 Confined in Nitrogen-Doped Nanoporous Carbon Frameworks. *Chemistry of Materials* **2018,** *30* (9), 2930-2938.
26. Carr, C. L.; Majzoub, E. H., Surface-Functionalized Nanoporous Carbons for Kinetically Stabilized Complex Hydrides through Lewis Acid–Lewis Base Chemistry. *The Journal of Physical Chemistry C* **2016,** *120* (21), 11426-11432.
27. Furukawa, H.; Cordova, K. E.; O'Keeffe, M.; Yaghi, O. M., The Chemistry and Applications of Metal-Organic Frameworks. *Science* **2013,** *341* (6149), 974-+.
28. Coudert, F.-X.; Fuchs, A. H., Computational characterization and prediction of metal–organic framework properties. *Coordination Chemistry Reviews* **2016,** *307*, 211-236.

29. Lim, D.-W.; Yoon, J. W.; Ryu, K. Y.; Suh, M. P., Magnesium Nanocrystals Embedded in a Metal–Organic Framework: Hybrid Hydrogen Storage with Synergistic Effect on Physi- and Chemisorption. *Angewandte Chemie International Edition* **2012,** *51* (39), 9814-9817.
30. Li, G.; Kobayashi, H.; Taylor, J. M.; Ikeda, R.; Kubota, Y.; Kato, K.; Takata, M.; Yamamoto, T.; Toh, S.; Matsumura, S.; Kitagawa, H., Hydrogen storage in Pd nanocrystals covered with a metal–organic framework. *Nature Materials* **2014,** *13*, 802.
31. Zlotea, C.; Campesi, R.; Cuevas, F.; Leroy, E.; Dibandjo, P.; Volkringer, C.; Loiseau, T.; Férey, G.; Latroche, M., Pd Nanoparticles Embedded into a Metal-Organic Framework: Synthesis, Structural Characteristics, and Hydrogen Sorption Properties. *Journal of the American Chemical Society* **2010,** *132* (9), 2991-2997.
32. Bhakta, R. K.; Herberg, J. L.; Jacobs, B.; Highley, A.; Behrens, R.; Ockwig, N. W.; Greathouse, J. A.; Allendorf, M. D., Metal−Organic Frameworks As Templates for Nanoscale NaAlH4. *Journal of the American Chemical Society* **2009,** *131* (37), 13198-13199.
33. Gonzalez, M. I.; Turkiewicz, A. B.; Darago, L. E.; Oktawiec, J.; Bustillo, K.; Grandjean, F.; Long, G. J.; Long, J. R., Confinement of atomically defined metal halide sheets in a metal–organic framework. *Nature* **2019,** *doi:10.1038/s41586-019-1776-0*.
34. Katz, M. J.; Brown, Z. J.; Colón, Y. J.; Siu, P. W.; Scheidt, K. A.; Snurr, R. Q.; Hupp, J. T.; Farha, O. K., A facile synthesis of UiO-66, UiO-67 and their derivatives. *Chemical Communications* **2013,** *49* (82), 9449-9451.
35. Madrahimov, S. T.; Gallagher, J. R.; Zhang, G.; Meinhart, Z.; Garibay, S. J.; Delferro, M.; Miller, J. T.; Farha, O. K.; Hupp, J. T.; Nguyen, S. T., Gas-Phase Dimerization of Ethylene under Mild Conditions Catalyzed by MOF Materials Containing (bpy)NiII Complexes. *ACS Catalysis* **2015,** *5* (11), 6713-6718.
36. Bloch, E. D.; Britt, D.; Lee, C.; Doonan, C. J.; Uribe-Romo, F. J.; Furukawa, H.; Long, J. R.; Yaghi, O. M., Metal Insertion in a Microporous Metal−Organic Framework Lined with 2,2′-Bipyridine. *Journal of the American Chemical Society* **2010,** *132* (41), 14382-14384.
37. Toyao, T.; Miyahara, K.; Fujiwaki, M.; Kim, T.-H.; Dohshi, S.; Horiuchi, Y.; Matsuoka, M., Immobilization of Cu Complex into Zr-Based MOF with Bipyridine Units for Heterogeneous Selective Oxidation. *The Journal of Physical Chemistry C* **2015,** *119* (15), 8131-8137.
38. Tu, T. N.; Nguyen, M. V.; Nguyen, H. L.; Yuliarto, B.; Cordova, K. E.; Demir, S., Designing bipyridine-functionalized zirconium metal–organic frameworks as a platform for clean energy and other emerging applications. *Coordination Chemistry Reviews* **2018,** *364*, 33-50.
39. Zavorotynska, O.; El-Kharbachi, A.; Deledda, S.; Hauback, B. C., Recent progress in magnesium borohydride Mg(BH4)2: Fundamentals and applications for energy storage. *International Journal of Hydrogen Energy* **2016,** *41* (32), 14387-14403.
40. Newhouse, R. J.; Stavila, V.; Hwang, S.-J.; Klebanoff, L. E.; Zhang, J. Z., Reversibility and Improved Hydrogen Release of Magnesium Borohydride. *The Journal of Physical Chemistry C* **2010,** *114* (11), 5224-5232.
41. Dimitrievska, M.; White, J. L.; Zhou, W.; Stavila, V.; Klebanoff, L. E.; Udovic, T. J., Structure-dependent vibrational dynamics of Mg(BH4)2 polymorphs probed with neutron vibrational spectroscopy and first-principles calculations. *Physical Chemistry Chemical Physics* **2016,** *18* (36), 25546-25552.
42. Soloveichik, G. L.; Gao, Y.; Rijssenbeek, J.; Andrus, M.; Kniajanski, S.; Bowman, R. C.; Hwang, S.-J.; Zhao, J.-C., Magnesium borohydride as a hydrogen storage material: Properties and dehydrogenation pathway of unsolvated Mg(BH4)2. *International Journal of Hydrogen Energy* **2009,** *34* (2), 916-928.
43. Matsunaga, T.; Buchter, F.; Miwa, K.; Towata, S.; Orimo, S.; Züttel, A., Magnesium borohydride: A new hydrogen storage material. *Renewable Energy* **2008,** *33* (2), 193-196.
44. Zhang, B.-S.; Qiu, J.-P.; Liu, L.-H.; Xu, W., Tetra-aqua-(2,2'-bipyridine-κN,N')magnesium(II) bis-(4-fluoro-benzoate). *Acta crystallographica. Section E, Structure reports online* **2010,** *66* (Pt 12), m1624-m1624.
45. Soloveichik, G.; Her, J.-H.; Stephens, P. W.; Gao, Y.; Rijssenbeek, J.; Andrus, M.; Zhao, J. C., Ammine Magnesium Borohydride Complex as a New Material for Hydrogen Storage: Structure and Properties of Mg(BH4)2·2NH3. *Inorganic Chemistry* **2008,** *47* (10), 4290-4298.

46. Manna, K.; Zhang, T.; Lin, W., Postsynthetic Metalation of Bipyridyl-Containing Metal–Organic Frameworks for Highly Efficient Catalytic Organic Transformations. *Journal of the American Chemical Society* **2014,** *136* (18), 6566-6569.
47. Zanella, P.; Crociani, L.; Masciocchi, N.; Giunchi, G., Facile High-Yield Synthesis of Pure, Crystalline Mg(BH4)2. *Inorganic Chemistry* **2007,** *46* (22), 9039-9041.
48. Fei, H.; Cohen, S. M., A robust, catalytic metal–organic framework with open 2,2′-bipyridine sites. *Chemical Communications* **2014,** *50* (37), 4810-4812.
49. Sugai, C.; Kim, S.; Severa, G.; White, J. L.; Leick, N.; Martinez, M. B.; Gennett, T.; Stavila, V.; Jensen, C., Kinetic Enhancement of Direct Hydrogenation of MgB2 to Mg(BH4)2 upon Mechanical Milling with THF, MgH2, and/or Mg. *ChemPhysChem* **2019,** *20* (10), 1301 - 1304.
50. Gallington, L. C.; Kim, I. S.; Liu, W.-G.; Yakovenko, A. A.; Platero-Prats, A. E.; Li, Z.; Wang, T. C.; Hupp, J. T.; Farha, O. K.; Truhlar, D. G.; Martinson, A. B. F.; Chapman, K. W., Regioselective Atomic Layer Deposition in Metal–Organic Frameworks Directed by Dispersion Interactions. *Journal of the American Chemical Society* **2016,** *138* (41), 13513-13516.
51. White, J. L.; Newhouse, R. J.; Zhang, J. Z.; Udovic, T. J.; Stavila, V., Understanding and Mitigating the Effects of Stable Dodecahydro-closo-dodecaborate Intermediates on Hydrogen-Storage Reactions. *The Journal of Physical Chemistry C* **2016,** *120* (45), 25725-25731.
52. Jensen, S. R. H.; Paskevicius, M.; Hansen, B. R. S.; Jakobsen, A. S.; Møller, K. T.; White, J. L.; Allendorf, M. D.; Stavila, V.; Skibsted, J.; Jensen, T. R., Hydrogenation properties of lithium and sodium hydride – closo-borate, [B10H10]2− and [B12H12]2−, composites. *Physical Chemistry Chemical Physics* **2018,** *20* (23), 16266-16275.
53. Wang, C.-A.; Han, Y.-F.; Li, Y.-W.; Nie, K.; Cheng, X.-L.; Zhang, J.-P., Bipyridyl palladium embedded porous organic polymer as highly efficient and reusable heterogeneous catalyst for Suzuki–Miyaura coupling reaction. *RSC Advances* **2016,** *6* (41), 34866-34871.
54. Broicher, C.; Foit, S. R.; Rose, M.; Hausoul, P. J. C.; Palkovits, R., A Bipyridine-Based Conjugated Microporous Polymer for the Ir-Catalyzed Dehydrogenation of Formic Acid. *ACS Catalysis* **2017,** *7* (12), 8413-8419.
55. Hug, S.; Stegbauer, L.; Oh, H.; Hirscher, M.; Lotsch, B. V., Nitrogen-Rich Covalent Triazine Frameworks as High-Performance Platforms for Selective Carbon Capture and Storage. *Chemistry of Materials* **2015,** *27* (23), 8001-8010.
56. Walter, E. D.; Qi, L.; Chamas, A.; Mehta, H. S.; Sears, J. A.; Scott, S. L.; Hoyt, D. W., Operando MAS NMR Reaction Studies at High Temperatures and Pressures. *The Journal of Physical Chemistry C* **2018,** *122* (15), 8209-8215.
57. Sinha, N.; Grant, C. V.; Wu, C. H.; De Angelis, A. A.; Howell, S. C.; Opella, S. J., SPINAL modulated decoupling in high field double- and triple-resonance solid-state NMR experiments on stationary samples. *Journal of Magnetic Resonance* **2005,** *177* (2), 197-202.
58. Giannozzi, P.; Baroni, S.; Bonini, N.; Calandra, M.; Car, R.; Cavazzoni, C.; Ceresoli, D.; Chiarotti, G. L.; Cococcioni, M.; Dabo, I.; Dal Corso, A.; de Gironcoli, S.; Fabris, S.; Fratesi, G.; Gebauer, R.; Gerstmann, U.; Gougoussis, C.; Kokalj, A.; Lazzeri, M.; Martin-Samos, L.; Marzari, N.; Mauri, F.; Mazzarello, R.; Paolini, S.; Pasquarello, A.; Paulatto, L.; Sbraccia, C.; Scandolo, S.; Sclauzero, G.; Seitsonen, A. P.; Smogunov, A.; Umari, P.; Wentzcovitch, R. M., QUANTUM ESPRESSO: a modular and open-source software project for quantum simulations of materials. *Journal of Physics: Condensed Matter* **2009,** *21* (39), 395502.
59. Giannozzi, P.; Andreussi, O.; Brumme, T.; Bunau, O.; Buongiorno Nardelli, M.; Calandra, M.; Car, R.; Cavazzoni, C.; Ceresoli, D.; Cococcioni, M.; Colonna, N.; Carnimeo, I.; Dal Corso, A.; de Gironcoli, S.; Delugas, P.; DiStasio, R. A.; Ferretti, A.; Floris, A.; Fratesi, G.; Fugallo, G.; Gebauer, R.; Gerstmann, U.; Giustino, F.; Gorni, T.; Jia, J.; Kawamura, M.; Ko, H. Y.; Kokalj, A.; Küçükbenli, E.; Lazzeri, M.; Marsili, M.; Marzari, N.; Mauri, F.; Nguyen, N. L.; Nguyen, H. V.; Otero-de-la-Roza, A.; Paulatto, L.; Poncé, S.; Rocca, D.; Sabatini, R.; Santra, B.; Schlipf, M.; Seitsonen, A. P.; Smogunov, A.; Timrov, I.; Thonhauser, T.; Umari, P.; Vast, N.; Wu, X.; Baroni, S., Advanced capabilities for materials modelling with Quantum ESPRESSO. *Journal of Physics: Condensed Matter* **2017,** *29* (46), 465901.

TOC Figure